Magnetoresistance Oscillations in Vertical Junctions of 2D Antiferromagnetic Semiconductor $CrPS_4$

Pengyuan Shi,[1,*] Xiaoyu Wang,[1,*] Lihao Zhang,[1] Wenqin Song,[2] Kunlin Yang,[2] Shuxi Wang,[1] Ruisheng Zhang,[1] Liangliang Zhang,[3] Takashi Taniguchi,[4] Kenji Watanabe,[5] Sen Yang,[1] Lei Zhang,[1] Lei Wang,[6] Wu Shi,[2,7] Jie Pan,[1,†] and Zhe Wang[1,‡]

[1]*MOE Key Laboratory for Nonequilibrium Synthesis and Modulation of Condensed Matter, Shaanxi Province Key Laboratory of Advanced Materials and Mesoscopic Physics, School of Physics, Xi'an Jiaotong University, Xi'an 710049, China*
[2]*State Key Laboratory of Surface Physics and Institute for Nanoelectronic Devices and Quantum Computing, Fudan University, Shanghai 200433, China*
[3]*State Key Laboratory for Manufacturing Systems Engineering, Xi'an Jiaotong University, Xi'an 710049, China*
[4]*Research Center for Materials Nanoarchitectonics, National Institute for Materials Science, 1-1 Namiki, Tsukuba 305-0044, Japan*
[5]*Research Center for Electronic and Optical Materials, National Institute for Materials Science, 1-1 Namiki, Tsukuba 305-0044, Japan*
[6]*Key Laboratory of Quantum Materials and Devices of Ministry of Education, School of Physics, Southeast University, 211189, Nanjing, China*
[7]*Zhangjiang Fudan International Innovation Center, Fudan University, Shanghai 201210, China*

(Received 14 April 2024; revised 26 October 2024; accepted 8 November 2024; published 13 December 2024)

Magnetoresistance (MR) oscillations serve as a hallmark of intrinsic quantum behavior, traditionally observed only in conducting systems. Here we report the discovery of MR oscillations in an insulating system, the vertical junctions of $CrPS_4$ which is a two-dimensional *A*-type antiferromagnetic semiconductor. Systematic investigations of MR peaks under varying conditions, including electrode materials, magnetic field direction, temperature, voltage bias, and layer number, elucidate a correlation between MR oscillations and spin-canted states in $CrPS_4$. Experimental data and analysis point out the important role of the in-gap electronic states in generating MR oscillations, and we propose that spin selected interlayer hopping of localized defect states may be responsible for it. Our findings not only illuminate the unusual electronic transport in $CrPS_4$ but also underscore the potential of van der Waals magnets for exploring interesting phenomena.

DOI: 10.1103/PhysRevX.14.041065 Subject Areas: Electronics, Spintronics

I. INTRODUCTION

Magnetoresistance (MR) is a phenomenon widely studied for its demonstration of intriguing physics and potential applications in industrial technologies. Magnetoresistance oscillation, characterized by nonmonotonic changes multitimes in resistance with respect to an external magnetic field, often manifests the inherent quantum mechanical nature of the studied system. The well-known examples include Shubnikov–de Haas oscillations, where the electron density of states on the Fermi surface varies with magnetic field, and Aharonov-Bohm effect, where the phase of conducting electrons shift by an external magnetic field [1]. However, these phenomena usually present in conducting systems, and observations of MR oscillations in insulating systems are rare.

MR of insulating magnetic systems actually has been a focus of research over the past decades, forming the foundation of spintronics, which has had a significant impact on current information technologies [2–4]. One classic model is the magnetic tunneling junction, consisting of two ferromagnetic metals separated by a thin insulator. Electron transport in such systems occurs via tunneling, where resistance depends on the alignment of electron magnetizations [2,4,5]. Another notable model is the spin filter of magnetic semiconductor, characterized by its spin-split band structure, thus leading to different tunneling

*These authors contributed equally to this work.
†Contact author: jiepan@xjtu.edu.cn
‡Contact author: zhe.wang@xjtu.edu.cn

barrier heights for different spins. After the pioneering works on Eu-based systems [6,7], recent advancements in 2D magnetic semiconductors [8–13], particularly in systems like CrI_3 [14–17], have demonstrated substantial progress in achieving large magnetoresistance. In both magnetic tunneling junctions and spin filters with magnetic semiconductor, MR oscillation is not expected as resistance typically correlates monotonically with the total magnetization of the system.

Here we report observations of MR oscillations in vertical junctions of 2D antiferromagnetic semiconductor $CrPS_4$. While the total magnetization of few-layer $CrPS_4$ is monotonically changed by magnetic field, several well-defined resistance peaks appear in the MR measurements. The MR oscillation is robust against different directions of applied magnetic field, and smoothly vanishes as the temperature goes above Néel temperature of $CrPS_4$. No MR oscillation is observed when the junction barrier is thinned down to monolayer, which is a ferromagnetic semiconductor. These findings demonstrate that the MR oscillations are correlated to the spin-canted states in the system. We further discuss the possible transport mechanism in $CrPS_4$ and point out that the in-gap states would play an important role.

II. EXPERIMENTAL RESULTS

$CrPS_4$ is a van der Waals layered semiconductor with band gap of around 1.3 eV [18–23], the structure of which is depicted in Fig. 1(a). Below the Néel temperature of 38 K [refer to Fig. 1(b)], Cr atoms within the *ab* plane of the crystal exhibit ferromagnetic coupling, while the interlayer coupling is antiferromagnetic [24–26], being *A*-type antiferromagnet. Upon the application of a magnetic field along the *c* axis, the spins undergo a spin-flop transition at approximately 0.7 T, followed by a smooth alignment along the direction of the magnetic field until reaching the saturation field of approximately 8.25 T.

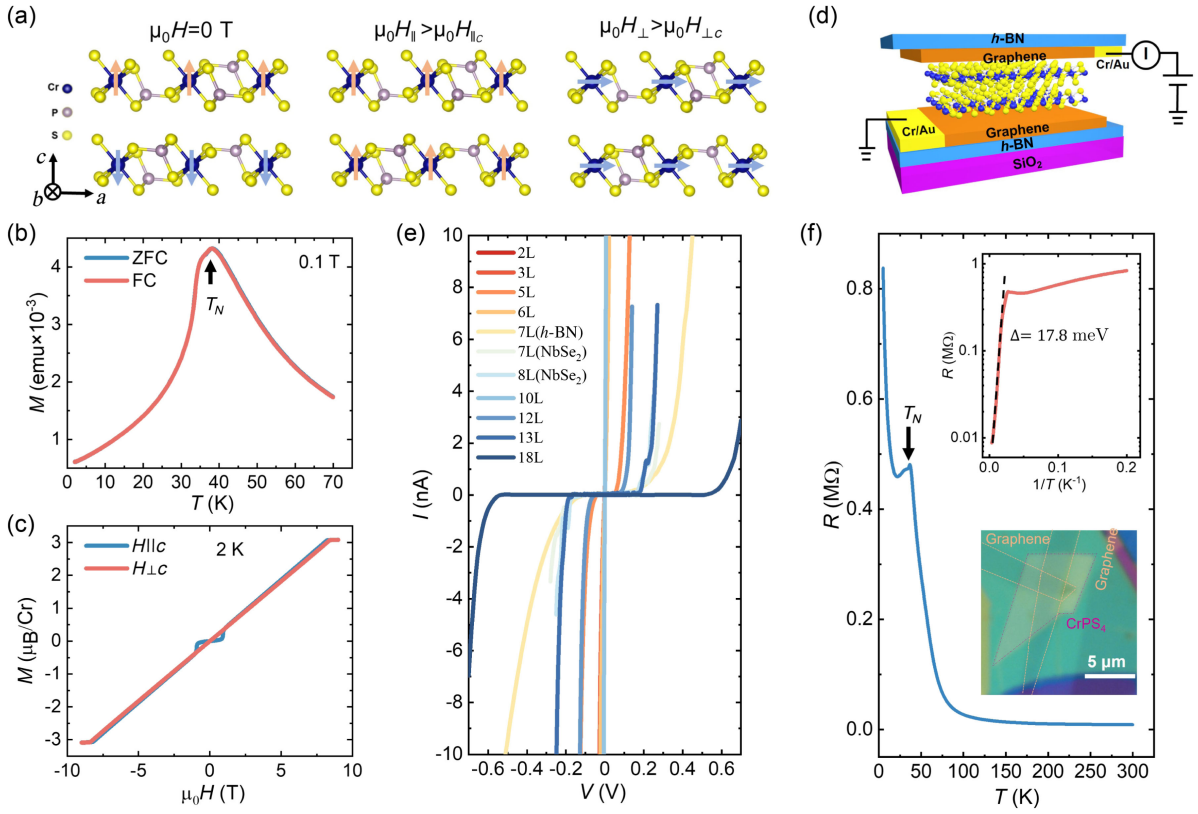

FIG. 1. Basic characteristics of bulk $CrPS_4$ and vertical junctions of few-layer $CrPS_4$. (a) Crystal and magnetic structure of $CrPS_4$, depicting its *A*-type antiferromagnetic behavior below the Néel temperature with the easy axis along the *c* axis. Above the spin-flip field, the magnetic moment aligns with the external magnetic field. (b) Temperature dependence of magnetization under zero-field-cooling (ZFC) and field-cooling (FC) conditions, indicating a Néel temperature of around 38 K. (c) Magnetic field dependence of magnetization with the magnetic field parallel and perpendicular to the *c* axis. (d) Schematic of vertical junctions, with graphene serving as electrodes and *h*-BN used to encapsulate the entire device. (e) *IV* curves of different vertical junctions at 2 K, all devices exhibiting very large resistivity. Here 7L(*h*-BN) denotes device with *h*-BN inserted between graphene and $CrPS_4$, 7L($NbSe_2$) and 8L($NbSe_2$) represent devices with $NbSe_2$ as electrodes. All other devices use graphene as electrodes. (f) Temperature dependence of resistance of a ten-layer device, with a kink clearly identified at the Néel temperature. The upper inset shows the Arrhenius plot, while the lower inset displays the optical image of the device.

Conversely, when the magnetic field is applied perpendicular to the c axis, no spin-flop transition occurs, and the magnetization increases smoothly with the magnetic field until reaching a saturation field of approximately 8.45 T, as shown in Fig. 1(c). These observations confirm the easy axis of $CrPS_4$ to be along the c axis, consistent with previous bulk measurements [25–27]. Based on the spin-flop transition field and the saturation field in two different directions, we estimate the interlayer coupling energy to be 0.16 meV and the on-site anisotropy energy to be 0.0045 meV, which are found to be very close to the neutron scattering measurement results [28]. This weak anisotropy energy results in similar spin-canted states for magnetic fields applied along both directions, as evidenced by nearly identical magnetization in both cases.

To investigate the electronic transport properties of few-layer $CrPS_4$, we fabricated vertical junctions of graphene/$CrPS_4$/graphene as illustrated in Fig. 1(d) (see the Appendix for details of fabrications). Figure 1(e) presents the IV curves of vertical junctions comprising multilayer $CrPS_4$ at 2 K. Some thicker devices exhibit clearly nonlinear IV behavior with ultrahigh resistivity at zero voltage bias. Devices exhibiting relatively linear IV behavior also demonstrate high resistivity, typically over 10^5 Ω cm. These findings indicate the insulating behavior of our devices at low temperatures, consistent with previous reports on both bulk and thin flakes of $CrPS_4$ [23,29–34]. We also fabricated a field-effect transistor to measure the longitudinal transport (see Supplemental Material Note 1 [35]); the resistance at zero gate voltage is very large and beyond our measurement capability. The insulating state is further corroborated by temperature-dependent resistance measurements, as depicted in Fig. 1(f). The resistance increases by approximately 2 orders of magnitude as the device is cooled from room temperature to 50 K. Analysis of the Arrhenius plot [inset in Fig. 1(f)] reveals a thermal activation energy of 17.8 meV. At lower temperatures, the deviation from thermal activation transport behavior suggests electron transport occurs via tunneling or hopping processes, which will be discussed in detail later. Notably, a distinct feature is observed at the Néel temperature in the R vs T curve of all devices, confirming the consistent quality of our atomically thin devices and bulk samples.

Having established that our devices exhibit insulating behavior at low temperatures, we proceeded to investigate their electronic transport behavior under the influence of a magnetic field. Figure 2(a) illustrates the MR of a ten-layer device, defined as $MR = (R_H - R_0)/R_0$, when a magnetic field is applied parallel to the c axis at 2 K. In the low magnetic field region, resistance undergoes a sudden change at approximately ±0.6 T, closely matching the spin-flop transition field of bulk $CrPS_4$. In the high magnetic field region, resistance saturates at around 8 T, aligning with the magnetic field at which the magnetization saturates, known as the spin-flip transition field. These observations underscore the correlation between the electronic transport behavior of few-layer vertical junctions and the magnetic states of $CrPS_4$.

MR oscillations are prominently observed in the intermediate magnetic field region between the spin-flop transition and the spin-flip transition. The MR exhibits three distinct peaks at around 2, 4.7, and 6.4 T, labeled as

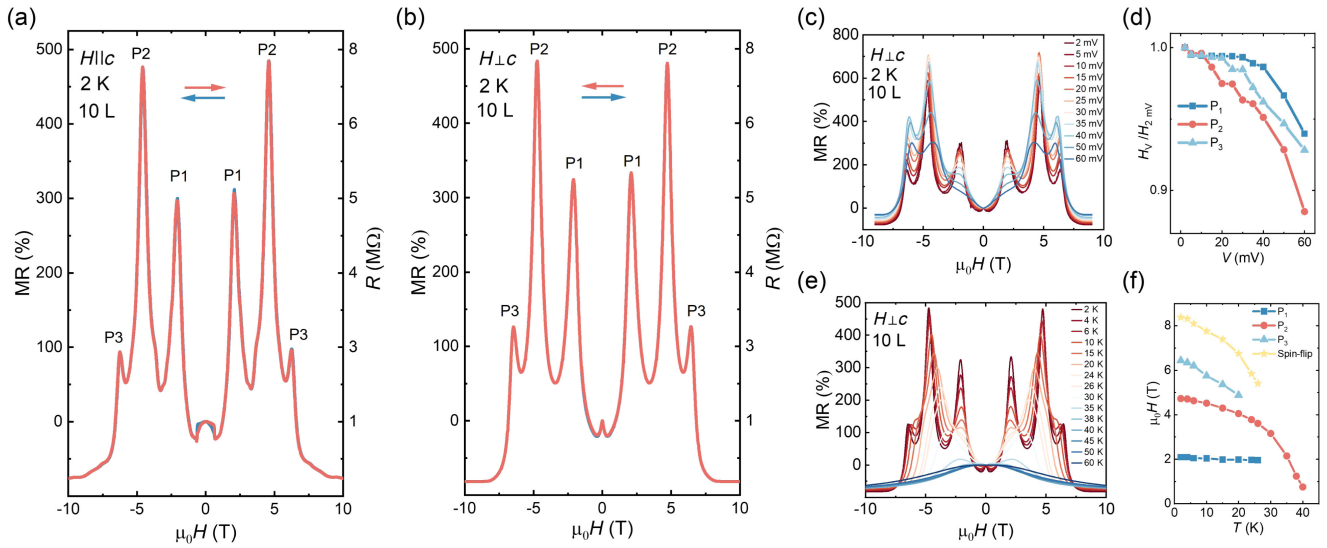

FIG. 2. MR oscillations in the vertical junction of ten-layer $CrPS_4$. (a) Magnetic field dependence of resistance measured with the field parallel to the c axis, obtained with a constant ac bias voltage of 2 mV at 2 K. Clear MR peaks are observed, along with the spin-flop transition at approximately ±0.6 T. (b) MR measured with the magnetic field perpendicular to the c axis. The persistence of MR oscillations indicates their origin from $CrPS_4$ rather than the graphene electrodes. (c) MR measured with different dc bias voltages. The MR peaks gradually shift to lower fields with increasing voltage, as summarized in (d). (e) MR at different temperatures measured with an ac bias voltage of 2 mV. The peak positions shift to lower fields as the temperature increases, as summarized in (f).

P1, P2, and P3, respectively. These peaks are evident in both magnetic field sweep directions and exhibit symmetry with respect to zero magnetic field. It is noteworthy that the magnetization of bulk $CrPS_4$ monotonically changes with the magnetic field, as previously demonstrated in Fig. 1(c). Similarly, the magnetization of few-layer flakes would also exhibit monotonic changes when considering the total magnetic energy of the system (see Supplemental Material Note 4 and Fig. 15(b) [35]), a behavior experimentally verified in various few layer *A*-type antiferromagnets [36,37]. In this context, the observation of MR oscillations in $CrPS_4$ vertical junctions is unexpected and stimulates further investigation.

One plausible explanation for these MR oscillations is a change in the density of states of the graphene electrodes induced by the perpendicular magnetic field. To explore this possibility, we conducted MR measurements with a magnetic field applied perpendicular to the *c* axis, and the corresponding data are presented in Fig. 2(b). In the low magnetic field region, the MR exhibited a smooth variation, as no spin-flop transition was anticipated when the magnetic field was perpendicular to the easy axis. In the high magnetic field region, the MR saturated at around 8.2 T, close to the bulk spin-flip transition field. Interestingly, in the intermediate magnetic field region, the MR oscillations remained largely unchanged in terms of both peak amplitudes and positions.

An alternative explanation is that the MR oscillations might originate from new states in the graphene electrodes induced by the proximity effect with magnet $CrPS_4$, persisting even when the magnetic field is perpendicular to the *c* axis. To test this hypothesis, We conducted two control experiments. First, we fabricated a device with the structure graphene/*h*-BN/$CrPS_4$/*h*-BN/graphene. The inclusion of thin *h*-BN layers between the graphene electrodes and $CrPS_4$ is intended to largely reduce the wave function overlap between them, thus eliminating any potential new states in graphene induced by proximity effect. Second, we constructed another type of device with the structure $NbSe_2/CrPS_4/NbSe_2$, where 2D metal $NbSe_2$ served as the electrodes, eliminating graphene entirely. As detailed in the Appendix, MR oscillations were clearly observed in both types of control devices.

These experiments provide robust evidence that the MR oscillations originated from $CrPS_4$ itself, rather than from the graphene electrodes. In the following we focus on the devices of graphene/$CrPS_4$/graphene. Figure 2(c) illustrates the MR measurements of ten-layer device conducted under different voltage biases at 2 K. The MR oscillations persisted across all measured biases, albeit with decreasing amplitudes as the bias increased. At a bias of 60 mV, the identification of the first peaks became less straightforward. Interestingly, the positions of the MR peaks shifted to lower magnetic fields with increasing bias, as summarized in Fig. 2(d).

We further investigated the temperature dependence of the MR behavior. As shown in Fig. 2(e), the amplitudes of the MR oscillations decreased with increasing temperature, ultimately vanishing at around 40 K, close to the Néel temperature of $CrPS_4$. In addition to affecting the amplitude of the MR oscillations, increasing temperature also shifted all three peaks to lower magnetic field, as summarized in Fig. 2(f). This temperature dependence contrasts with that of typical quantum MR oscillations observed in conducting systems, such as Shubnikov–de Haas oscillations and the Aharonov-Bohm effect, where MR peak positions remain independent of temperature. The similar trend in temperature dependence between the MR oscillations and the spin-flip transition suggests a connection to the canted magnetic states of $CrPS_4$.

Before delving deeper into the origin of MR oscillations, we investigated this behavior in devices with varying thicknesses. Figure 3(a) presents the MR of 12-layer device, characterized by a clearly nonlinear *IV* curve, indicative of even more insulating compared to ten-layer device. Three MR peaks are distinctly observed in both perpendicular and parallel magnetic field configurations, with the middle peak (P2) dominating in comparison to ten-layer device. Turning to the results of the six-layer device, as shown in Fig. 3(b), only two MR peaks are observed in most measurements, with an additional small MR peak emerging when the voltage is less than 5 mV (see Supplemental Material Fig. 9 [35]). This specific flake has clear crystal crossed with angle of 67.5°, meaning the crystal edge is a crystal axis [25,38], as indicated in the inset of Fig. 3(b). We applied the magnetic field along this axis, and the measured MR is almost the same as the result of randomly applied in-plane field.

We have measured total 11 multilayer devices and Figs. 3(c) and 3(d) summarize the featured magnetic fields of all devices (see Supplemental Material for additional electronic transport data of devices [35]). Figure 3(c) illustrates MR peak positions measured under various voltages at 2 K, where each color represents data from one device and each symbol denotes the same peak in that device. It is evident that all MR peaks shift to lower magnetic fields with increasing voltage, and they can be roughly divided into four groups. Figure 3(d) depicts the thickness dependence of the spin-flip field. The dots represent data obtained from the saturation of magnetoconductance in the parallel field configuration, particularly the bilayer and three-layer device reveals a clear decrease. This reduction aligns with expectations, as the effective interlayer coupling energy per layer decreases. This phenomenon can be fully elucidated using the antiferromagnetic linear chain model, as discussed in the Supplemental Material [35].

Expanding our investigation to the atomically thin limit, we studied monolayer $CrPS_4$, which has been identified as a ferromagnet [25]. Its zero-field temperature dependence

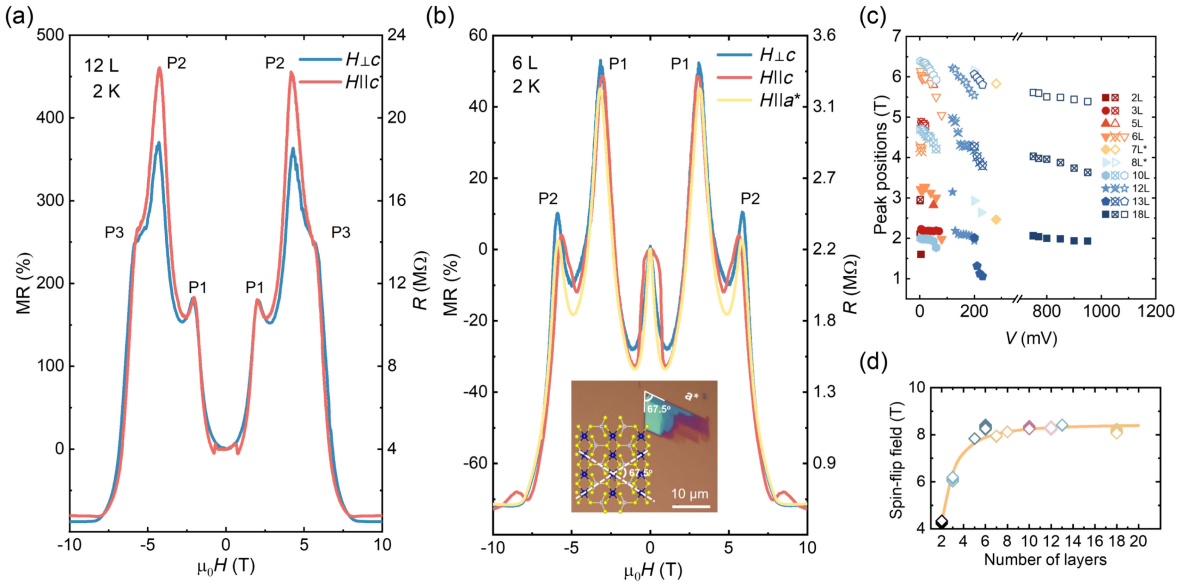

FIG. 3. Statistics of MR oscillations in few-layer $CrPS_4$ devices. (a) MR of a 12-layer device measured with a dc bias voltage of 0.15 V. Despite being more resistive than the ten-layer device, MR peaks persist in both magnetic field orientations. (b) MR of a six-layer device measured with an ac bias voltage of 10 mV. The inset shows the optical image of the flake, with the vertical junction located at the black point. The flake exhibits two sharp edges intersecting at an angle of 67.5°. Magnetic fields are applied parallel to the c axis, ab plane, and a^* axis. (c) Summary of MR peak positions for all few-layer devices. Here the seven- and eight-layer devices use $NbSe_2$ as electrodes. (d) Spin-flip transition fields determined from in-plane MR measurements at 2 K, with the solid line representing calculated results based on parameters derived from bulk magnetization data. The layer number is determined using a combination of atomic force microscopy and optical contrast, with approximate ±1 layer error for thick $CrPS_4$ flakes.

of resistance monotonic increase deviated at around 38 K [the arrow in Fig. 4(a)], which is around the same as the Néel temperature of bulk $CrPS_4$ [25,34,38]. Figure 4(b) presents measurement results with a magnetic field perpendicular to the c axis, where no MR oscillations are observed in this monolayer device. The MR is around zero at 2 K and becomes negative as temperature rises. The MR amplitude increases as temperature rises and reaches maximum at around Curie temperature, exhibiting a clear triangle shape when plotted as a function of temperature in a 2D format (see Supplemental Material [35]).

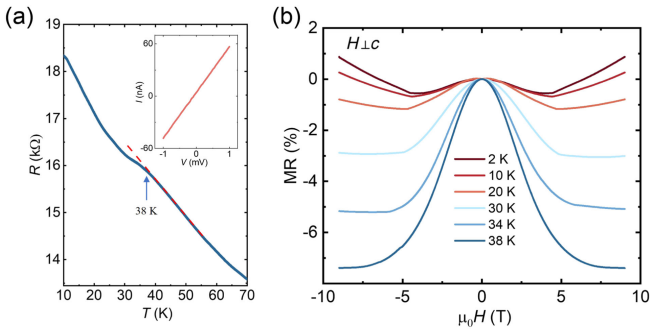

FIG. 4. Absence of MR oscillations in ferromagnetic monolayer $CrPS_4$ device. (a) Temperature dependence of resistance at zero field. The inset shows the IV curve of this vertical junction. (b) MR at different temperatures, measured with a magnetic field perpendicular to the c axis; no MR oscillation is observed.

This behavior closely resembles that observed in vertical junctions of other 2D ferromagnetic semiconductors, such as $CrBr_3$ [39] and monolayer CrSBr [40]. In contrast to antiferromagnets, no spin-canted states are expected in ferromagnets. The absence of MR oscillations in the monolayer device thus further confirms that the oscillatory behavior is related to spin-canted states.

III. DISCUSSION

In summary of the aforementioned experimental investigations across various devices, no MR oscillations are observed in monolayer device due to its ferromagnetic nature. Conversely, for antiferromagnetic few-layer devices, MR oscillations occur within the region between spin-flop and spin-flip transitions, with peak positions shifting in tandem with the spin-flip transition. These findings strongly suggest that MR oscillations are intricately linked to the magnetic canted states induced by the applied magnetic field.

To gain deeper insights into the specifics of these canted states in multilayer $CrPS_4$, we employ the antiferromagnetic linear-chain model [36,37]. Within this framework, the magnetization of each $CrPS_4$ layer is depicted as a macrospin with an on-site anisotropy energy K, coupled to its nearest neighbors through the interlayer coupling J. The magnetic state under a certain magnetic field can be elucidated by minimizing the total magnetic energy of the

system (detailed in Supplemental Material Notes 3 and 4 [35]). This model can nicely describe the layer number dependence of spin-flip field shown in Fig. 3(d), where the solid orange line represents the calculated results with parameters derived from bulk magnetization measurements. Our analysis reveals that while the total magnetization monotonically increases [Supplemental Material Fig. 15(b)], the canting angle undergoes nonmonotonic changes as a function of the magnetic field, for example, the canting angle of layer 2 and 5 in the six-layer $CrPS_4$ [Supplemental Material Fig. 15(a)].

Despite our insights into the magnetic states through the antiferromagnetic linear-chain model, establishing the link between the magnetic states and electronic transport proves elusive. Our calculations of MR based on the tunneling model used in $CrCl_3$ (see details in Supplemental Material Note 4 [35]) reveal a monotonic behavior, with no oscillations observed. This points out the importance of evaluating the predominant transport mechanism in vertical junctions of $CrPS_4$. Our analysis of the saturation of low-temperature resistance in the Arrhenius plot [see the inset of Fig. 1(f)] suggests that thermally activated electrons are not the predominant carriers within the examined temperature range. These imply the presence of states inside the gap of $CrPS_4$. This conclusion is also consistent with previous report on field-effect transistors of $CrPS_4$ [30], where only monotonic MR is observed when the Fermi level is tuned into the bands of $CrPS_4$, as the transport is not mediated by the in-gap states.

The nature of these in-gap states remains elusive. Previous observations of quantum MR oscillations in Kondo insulator YbB_{12} and topological insulator WTe_2 suggest an unconventional Fermi surface inside the insulating gap [41,42], yet their origins remain inconclusive. These oscillations, resembling Shubnikov–de Haas oscillations in metals, differ from those in our device, and the band gap opening mechanism in these systems also differs from $CrPS_4$. Besides the possibility of these exotic states, defects offer a trivial explanation for in-gap states in our devices. At high temperatures, hopping between defect states leads to thermally active behavior, with the activation barrier determined by the energy spacing between these states [43,44]. This scenario elucidates the ultrasmall thermal activation energy (17.8 meV) obtained from the Arrhenius plot, notably lower than the band gap (1.3 eV) of $CrPS_4$. With these defect states, variable-range hopping typically dominates at low temperatures in standard longitudinal devices [43,45]. However, given the small distance between the two graphene electrodes of our vertical junctions (few nanometers), direct application of classic variable-range hopping theory is untenable. Nevertheless, we can conceptualize the transport process in a similar manner, where electrons tunnel from one defect state to another suitable defect state, either within the same layer or in neighboring layers, until they reach the graphene electrode on the opposite side. The average hopping length is determined not only by the sample thickness but also by the defect density and the energy difference between these defects, potentially explaining why some thicker devices exhibit smaller resistance than thinner devices.

To further investigate the correlation between the electronic transport properties and the magnetic states in $CrPS_4$, we calculated the band structure of $CrPS_4$ containing sulfur (S) vacancies, a common type of defect in 2D transition metal chalcogenides. As detailed in the Supplemental Material [35], our calculations reveal localized states within the band gap of $CrPS_4$. Notably, the S vacancy is spin polarized, aligning with the spin direction of the Cr atoms in the layer. In the antiferromagnetic ground state, the substantial energy difference between spin-polarized defect states in adjacent layers (when considering spin conserved hopping) necessitates electron hopping to more distant layers, which increases the hopping length and, consequently, the resistance. When an external magnetic field is applied, spin canting reduces the energy difference between neighboring layers, facilitating hopping and thereby reducing the hopping length and the resistance. Concurrently, within conventional theory of hopping conduction in a magnetic field [45], the magnetic field compresses the wave function of the localized states, decreasing the probability of hopping and thus increasing the hopping length and resistance [46]. The interplay between these competing effects—spin canting and wave function contraction—accounts for the MR peaks observed in our measurements. Additionally, the application of an electric field can effectively reduce the energy difference between defect states, leading to a decrease in the hopping length [47–49]. This dependence on electric field strength modulates the competition between the spin-canting effect and the magnetic field effect, resulting in shifts in the positions of the MR peaks.

The interlayer hopping of spin-polarized defect states in $CrPS_4$ offers a plausible framework to quantitatively explain our key findings. We employed principles of conventional variable-range hopping theory to develop a toy model, the spin selected interlayer hopping model as detailed in the Supplemental Material [35], to calculate the MR. This model successfully captures the MR peaks and their shifts under an electric field. However, it does not accurately predict the peak positions observed in the experimental results. The exact MR oscillations' behavior, such as the MR magnitudes and peak positions, are influenced by the intricate behavior of the localized wave function in response to the magnetic field, as well as detailed calculations of hopping resistance. It is important to note that a comprehensive theory of interlayer hopping involving spin-polarized states in $2+1$ dimensions—considering the strong anisotropy along the c axis in our system—has yet to be developed. Further efforts are needed to clarify the exact nature of the in-gap states and to

establish a complete hopping conduction framework for such systems if spin-polarized defect states are indeed found to be responsible for the observed MR oscillations. At the same time, we note that the position of MR peaks can be more precisely described when we consider the interference between spin Berry phases. In the simplified scenario, the spin can follow two distinct evolutionary paths in a single hopping process due to the coexistence of spin-up and spin-down channels. Different spin Berry phases emerge for each of these cyclic quantum evolution paths [50]. The interference between these two paths, which is strongly dependent on the spin-canting configuration, further affects the overall hopping probability as detailed in the Supplemental Material. However, more efforts are needed to further support the existence of spin Berry phase coherence and investigate its precise origin [51].

IV. SUMMARY

In conclusion, our study reveals the presence of robust MR oscillations in vertical junctions of few-layer $CrPS_4$. These oscillations persist regardless of the direction of the applied magnetic field, whether parallel or perpendicular to the c axis. They are observed across a spectrum of samples, ranging from highly insulating (exhibiting clearly nonlinear IV curves with unmeasurable resistance at zero voltage bias) to those with relatively lower resistance (still in the order of megohm), as long as the device comprises multilayer $CrPS_4$. Moreover, the MR peaks exhibit a gradual shift to lower magnetic fields as the temperature increases, ultimately disappearing above the Néel temperature, mirroring the behavior of the spin-flip transition. This correlation underscores the connection between these MR oscillations and the canted magnetic state in $CrPS_4$. While further investigations are necessary to precisely determine the proposed spin-polarized defect states and possible coherence between spin Berry phase, our findings highlight $CrPS_4$ as a unique example of MR oscillations, a phenomenon rarely observed in insulating systems. This work underscores the potential of 2D van der Waals magnets not only for spintronics applications but also as intriguing platforms for exploring novel physics.

Note added in proof. Recently, we became aware of similar works [51,52].

ACKNOWLEDGMENTS

This work is financially supported by National Natural Science Foundation of China (Grants No. 12374121, No. 12304232, No. 12274090, and No. 92265103), Shaanxi Fundamental Science Research Project for Mathematics and Physics (22JSY026, 23JSQ011), Natural Science Basic Research Program of Shaanxi (2022JC-DW5-02), the Fundamental Research Funds for the Central Universities, and the Natural Science Foundation of Shanghai (Grant No. 22ZR1406300). S. Y. acknowledge support from the National Key Research and Development Program of China (2022YFE0109500). K. W. and T. T. acknowledge support from the JSPS KAKENHI (Grants No. 20H00354 and No. 23H02052) and World Premier International Research Center Initiative (WPI), MEXT, Japan.

APPENDIX

1. Bulk crystal growth and characterizations

$CrPS_4$ crystals were grown using the chemical vapor transport method, following established protocols [53]. Chromium, red phosphorus, and sulfur powders were measured stoichiometrically ($Cr:P:S = 1:1:4$) with 5% additional sulfur added as transport agent. The precursors were mixed and sealed into quartz ampoules under vacuum (10^{-2} Pa), followed by loading into a two-zone furnace. The hot and cold ends of the ampoules were kept at 680 °C and 600 °C, respectively, for 8 days. At the end of the growth process, the furnace was turned off for natural cooling and the $CrPS_4$ crystals could be collected from the cold zone of the ampoule. X-ray diffraction was performed to determine the structure of the grown crystals. One crystal weighing 1.13 mg was utilized for magnetization measurements performed in a physical property measurement system (PPMS) VSM magnetometer (Quantum Design), with the magnetic field oriented parallel or perpendicular to the crystallographic c-axis.

2. Vertical junction fabrication and transport measurements

Atomically thin $CrPS_4$ flakes were obtained through mechanical exfoliation from bulk crystals. The vertical junctions of graphene/$CrPS_4$/graphene were assembled using a standard pickup technique with stamps of polydimethylsiloxane(PDMS)/polycarbonate(PC). To ensure the high quality of the vertical junctions, exfoliation and assembly were conducted within a glove box filled with nitrogen gas, and the junctions were encapsulated with h-BN. Standard nanofabrication processes, including electron beam lithography, reactive ion etching, and electron beam evaporation (10 nm/50 nm Cr/Au), were employed to make contacts to the graphene electrodes. Electronic transport measurements were conducted in a cryostat from Cryogenic or PPMS from Quantum Design, using a Keithley 2400 and SR830 lock-in amplifier. MR of multilayer devices were measured with constant bias voltage, and the monolayer device was measured with constant current of 40 nA. Frequency of 17.773 Hz was used in ac measurements.

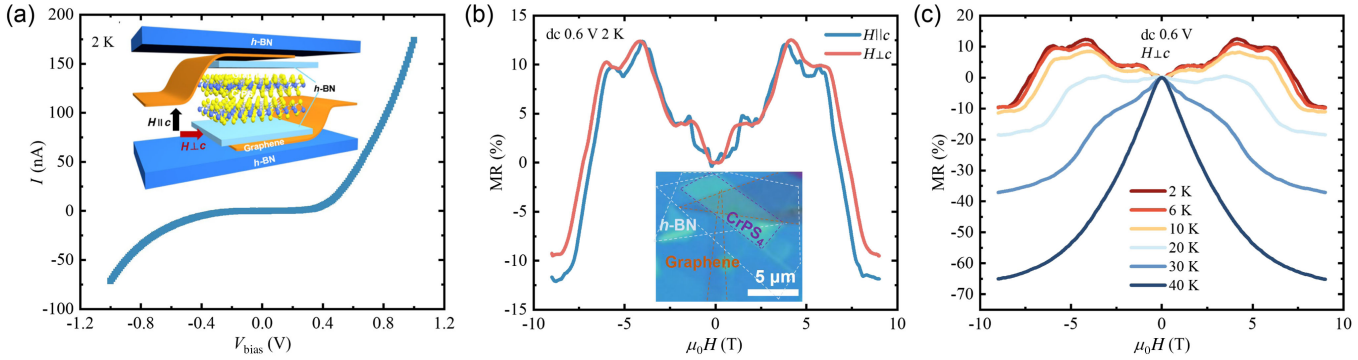

FIG. 5. MR oscillations in vertical junction of graphene/*h*-BN/$CrPS_4$/*h*-BN/graphene. (a) *IV* curve of the device at 2 K and zero field, the difference thickness of inserted *h*-BN results in the asymmetry of the device. The inset shows schematic of vertical junction graphene/*h*-BN/$CrPS_4$/*h*-BN/graphene, where thin *h*-BN was inserted between graphene electrodes and $CrPS_4$. (b) MR oscillations at 2 K with magnetic field applied parallel and perpendicular to the *c* axis. The measurement is done with constant dc voltage of 0.6 V. The inset shows the optical image of the device. (c) MR at different temperatures; the magnetic field is applied perpendicular to *c* axis.

3. Electronic transport data of vertical junctions with different electrodes

As discussed in the main text, one possible explanation of MR oscillations is that they might originate from new states in the graphene electrodes induced by the proximity effect with magnet $CrPS_4$. To address this, we conducted two control experiments. First, we fabricated a device with the structure graphene/*h*-BN/$CrPS_4$/*h*-BN/graphene. The proximity effect typically involves the expansion of the wave function from one material into another, resulting in new properties in the latter. This wave function expansion decreases exponentially with increasing distance between the materials. For instance, ferromagnetism in graphene induced by proximity to a yttrium iron garnet (YIG) substrate disappears when a very thin Al_2O_3 layer is inserted between them [54]. In our device, the thin *h*-BN layer inserted between $CrPS_4$ and graphene would eliminate any potential new states in graphene induced by proximity to $CrPS_4$. As shown in Fig. 5, MR oscillations

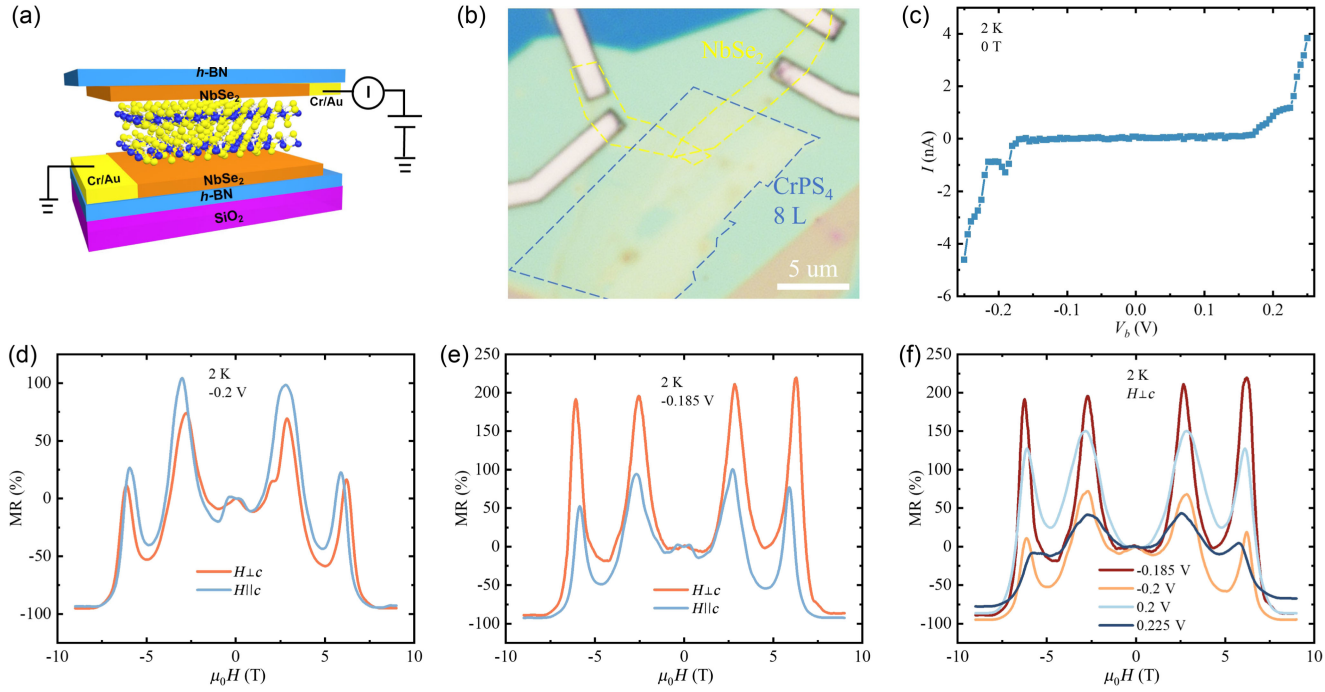

FIG. 6. MR oscillations in vertical junction of $NbSe_2/CrPS_4/NbSe_2$. (a) Schematic of vertical junction $NbSe_2/CrPS_4/NbSe_2$. (b) Optical image of device NS1. (c) *IV* curve measured at 2 K at zero magnetic field. (d) MR oscillation at 2 K with magnetic field parallel and perpendicular to the *c* axis. Applied dc bias voltage is −0.2 V. (e) MR oscillation at 2 K with dc bias voltage −0.185 V. (f) MR oscillation at 2 K with different dc bias voltage; magnetic field is perpendicular to *c* axis.

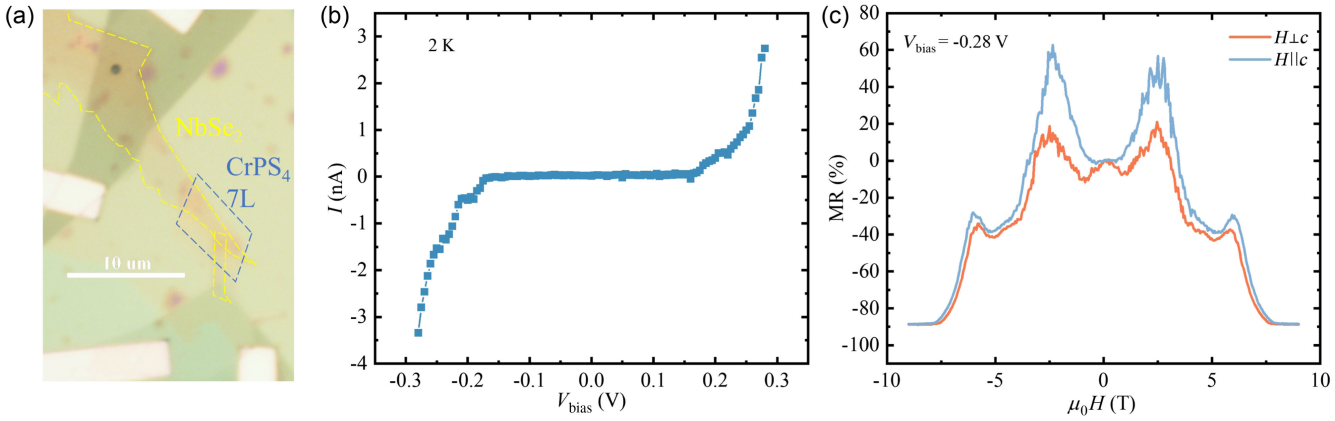

FIG. 7. MR oscillations in another vertical junction of $NbSe_2/CrPS_4/NbSe_2$. (a) Optical image of device NS2. (b) IV curve measure at 2 K at zero magnetic field. (c) MR oscillation at 2 K with magnetic field parallel and perpendicular to the c axis. Applied dc bias voltage is −0.28 V.

were still clearly observed when magnetic field was applied parallel or perpendicular to the c axis of the device, providing evidence that these oscillations originate from $CrPS_4$ itself.

Second, we constructed another type of device with the structure $NbSe_2/CrPS_4/NbSe_2$ as illustrated in Fig. 6(a). We use 2D metal $NbSe_2$ as the electrodes and omit graphene in this type of device. The fabrication process for this device was similar to that described in the main text for the graphene/$CrPS_4$/graphene device. To avoid the oxidation of $NbSe_2$, the device was immediately loaded into the e-beam evaporator's vacuum chamber after etching the h-BN, with $NbSe_2$ exposure to air minimized to less than one minute. Figure 6 shows the results for one such device, NS1. The nonlinear IV curve at 2 K and 0 T is presented in Fig. 6(c). We observed features around ±0.2 V in the IV curve, which were also seen in another $NbSe_2/CrPS_4/NbSe_2$ device NS2, though their origin is unclear. Figures 6(d) and 6(e) show the MR at 2 K measured with biases of −0.2 and −0.185 V, respectively, where MR oscillations are evident. Figure 6(f) shows the MR at 2 K measured with both positive and negative biases, with the magnetic field applied perpendicular to the c axis, and MR oscillations are observed in all measurements.

For another $NbSe_2/CrPS_4/NbSe_2$ device, NS2, we used graphene flakes to make contacts to $NbSe_2$, ensuring $NbSe_2$ did not need to be exposed to air during fabrication (note that graphene did not contact $CrPS_4$). The results were very similar to those for device NS1, as shown in Fig. 7. The consistent data from one graphene/h-BN/CrPS4/h-BN/graphene device and two $NbSe_2/CrPS_4/NbSe_2$ devices provide robust evidence that the MR oscillations originate from the magnetic semiconductor $CrPS_4$ itself.

[1] N. W. Ashcroft and N. D. Mermin, *Solid State Physics*, College Ed. (Thomson Learning Inc., New York, 1976).

[2] I. Žutić, J. Fabian, and S. Das Sarma, *Spintronics: Fundamentals and applications*, Rev. Mod. Phys. **76**, 323 (2004).

[3] A. Avsar, H. Ochoa, F. Guinea, B. Ozyilmaz, B. J. van Wees, and I. J. Vera-Marun, *Colloquium: Spintronics in graphene and other two-dimensional materials*, Rev. Mod. Phys. **92**, 021003 (2020).

[4] A. Hirohata, K. Yamada, Y. Nakatani, I. L. Prejbeanu, B. Diény, P. Pirro, and B. Hillebrands, *Review on spintronics: Principles and device applications*, J. Magn. Magn. Mater. **509**, 166711 (2020).

[5] E. Y. Tsymbal, O. N. Mryasov, and P. R. LeClair, *Spin-dependent tunnelling in magnetic tunnel junctions*, J. Phys. Condens. Matter **15**, R109 (2003).

[6] G.-X. Miao, M. Müller, and J. S. Moodera, *Magnetoresistance in double spin filter tunnel junctions with nonmagnetic electrodes and its unconventional bias dependence*, Phys. Rev. Lett. **102**, 076601 (2009).

[7] T. S. Santos, J. S. Moodera, K. V. Raman, E. Negusse, J. Holroyd, J. Dvorak, M. Liberati, Y. U. Idzerda, and E. Arenholz, *Determining exchange splitting in a magnetic semiconductor by spin-filter tunneling*, Phys. Rev. Lett. **101**, 147201 (2008).

[8] K. S. Burch, D. Mandrus, and J.-G. Park, *Magnetism in two-dimensional van der Waals materials*, Nature (London) **563**, 47 (2018).

[9] K. F. Mak, J. Shan, and D. Ralph, *Probing and controlling magnetic states in 2D layered magnetic materials*, Nat. Rev. Phys. **1**, 646 (2019).

[10] C. Gong and X. Zhang, *Two-dimensional magnetic crystals and emergent heterostructure devices*, Science **363**, eaav4450 (2019).

[11] M. Gibertini, M. Koperski, A. F. Morpurgo, and K. S. Novoselov, *Magnetic 2D materials and heterostructures*, Nat. Nanotechnol. **14**, 408 (2019).

[12] B. Huang, M. A. McGuire, A. F. May, D. Xiao, P. Jarillo-Herrero, and X. Xu, *Emergent phenomena and proximity effects in two-dimensional magnets and heterostructures*, Nat. Mater. **19**, 1276 (2020).

[13] C. Boix-Constant, S. Jenkins, R. Rama-Eiroa, E. J. G. Santos, S. Mañas-Valero, and E. Coronado, *Multistep*

magnetization switching in orthogonally twisted ferromagnetic monolayers, Nat. Mater. **23**, 212 (2024).

[14] T. Song *et al.*, *Giant tunneling magnetoresistance in spin-filter van der Waals heterostructures*, Science **360**, 1214 (2018).

[15] D. R. Klein *et al.*, *Probing magnetism in 2D van der Waals crystalline insulators via electron tunneling*, Science **360**, 1218 (2018).

[16] Z. Wang, I. Gutiérrez-Lezama, N. Ubrig, M. Kroner, M. Gibertini, T. Taniguchi, K. Watanabe, A. Imamoğlu, E. Giannini, and A. F. Morpurgo, *Very large tunneling magnetoresistance in layered magnetic semiconductor* CrI_3, Nat. Commun. **9**, 2516 (2018).

[17] H. H. Kim, B. Yang, T. Patel, F. Sfigakis, C. Li, S. Tian, H. Lei, and A. W. Tsen, *One million percent tunnel magnetoresistance in a magnetic van der Waals heterostructure*, Nano Lett. **18**, 4885 (2018).

[18] A. Louisy, G. Ouvrard, D. Schleich, and R. Brec, *Physical properties and lithium intercalates of* $CrPS_4$, Solid State Commun. **28**, 61 (1978).

[19] P. Gu *et al.*, *Photoluminescent quantum interference in a van der Waals magnet preserved by symmetry breaking*, ACS Nano **14**, 1003 (2020).

[20] Q. L. Pei *et al.*, *Spin dynamics, electronic, and thermal transport properties of two-dimensional* $CrPS_4$ *single crystal*, J. Appl. Phys. **119**, 043902 (2016).

[21] H. L. Zhuang and J. Zhou, *Density functional theory study of bulk and single-layer magnetic semiconductor* $CrPS_4$, Phys. Rev. B **94**, 195307 (2016).

[22] J. Deng, J. Guo, H. Hosono, T. Ying, and X. Chen, *Two-dimensional bipolar ferromagnetic semiconductors from layered antiferromagnets*, Phys. Rev. Mater. **5**, 034005 (2021).

[23] R. A. Susilo *et al.*, *Band gap crossover and insulator–metal transition in the compressed layered* $CrPS_4$, npj Quantum Mater. **5**, 58 (2020).

[24] S. L. Bud'ko, E. Gati, T. J. Slade, and P. C. Canfield, *Magnetic order in the van der Waals antiferromagnet* $CrPS_4$*: Anisotropic h-t phase diagrams and effects of pressure*, Phys. Rev. B **103**, 224407 (2021).

[25] J. Son *et al.*, *Air-stable and layer-dependent ferromagnetism in atomically thin van der Waals* $CrPS_4$, ACS Nano **15**, 16904 (2021).

[26] Y. Peng *et al.*, *Magnetic structure and metamagnetic transitions in the van der Waals antiferromagnet* $CrPS_4$, Adv. Mater. **32**, 2001200 (2020).

[27] Y. Peng *et al.*, *Controlling spin orientation and metamagnetic transitions in anisotropic van der Waals antiferromagnet* $CrPs_4$ *by hydrostatic pressure*, Adv. Funct. Mater. **32**, 2106592 (2022).

[28] S. Calder, A. V. Haglund, Y. Liu, D. M. Pajerowski, H. B. Cao, T. J. Williams, V. O. Garlea, and D. Mandrus, *Magnetic structure and exchange interactions in the layered semiconductor* $CrPS_4$, Phys. Rev. B **102**, 024408 (2020).

[29] J. Yang *et al.*, *Layer-dependent giant magnetoresistance in two-dimensional* $CrPS_4$ *magnetic tunnel junctions*, Phys. Rev. Appl. **16**, 024011 (2021).

[30] F. Wu, M. Gibertini, K. Watanabe, T. Taniguchi, I. Gutiérrez-Lezama, N. Ubrig, and A. F. Morpurgo, *Gate-controlled magnetotransport and electrostatic modulation of magnetism in 2D magnetic semiconductor* $CrPS_4$, Adv. Mater. **35**, 2211653 (2023).

[31] F. Wu, M. Gibertini, K. Watanabe, T. Taniguchi, I. Gutiérrez-Lezama, N. Ubrig, and A. F. Morpurgo, *Magnetism-induced band-edge shift as the mechanism for magnetoconductance in* $CrPS_4$ *transistors*, Nano Lett. **23**, 8140 (2023).

[32] S. Qi *et al.*, *Giant electrically tunable magnon transport anisotropy in a van der Waals antiferromagnetic insulator*, Nat. Commun. **14**, 2526 (2023).

[33] D. K. de Wal, A. Iwens, T. Liu, P. Tang, G. E. W. Bauer, and B. J. van Wees, *Long-distance magnon transport in the van der Waals antiferromagnet* $CrPs_4$, Phys. Rev. B **107**, L180403 (2023).

[34] M. Huang *et al.*, *Layer-dependent magnetism and spin fluctuations in atomically thin van der Waals magnet* $CrPS_4$, Nano Lett. **23**, 8099 (2023).

[35] See Supplemental Material at http://link.aps.org/supplemental/10.1103/PhysRevX.14.041065 for basic characterizations of bulk crystals and thin flakes, additional electronic transport data of vertical junctions, calculations of defect states, and magnetoresistance based on spin selected interlayer hopping model.

[36] Z. Wang, M. Gibertini, D. Dumcenco, T. Taniguchi, K. Watanabe, E. Giannini, and A. F. Morpurgo, *Determining the phase diagram of atomically thin layered antiferromagnet* $CrCl_3$, Nat. Nanotechnol. **14**, 1116 (2019).

[37] S. Yang *et al.*, *Odd-even layer-number effect and layer-dependent magnetic phase diagrams in* $MnBi_2Te_4$, Phys. Rev. X **11**, 011003 (2021).

[38] J. Lee *et al.*, *Structural and optical properties of single- and few-layer magnetic semiconductor* $CrPS_4$, ACS Nano **11**, 10935 (2017).

[39] Z. Wang, I. Gutiérrez-Lezama, D. Dumcenco, N. Ubrig, T. Taniguchi, K. Watanabe, E. Giannini, M. Gibertini, and A. F. Morpurgo, *Magnetization dependent tunneling conductance of ferromagnetic barriers*, Nat. Commun. **12**, 6659 (2021).

[40] C. Boix-Constant, S. Mañas-Valero, A. M. Ruiz, A. Rybakov, K. A. Konieczny, S. Pillet, J. J. Baldoví, and E. Coronado, *Probing the spin dimensionality in single-layer* CrSBr *van der Waals heterostructures by magneto-transport measurements*, Adv. Mater. **34**, 2204940 (2022).

[41] Z. Xiang *et al.*, *Quantum oscillations of electrical resistivity in an insulator*, Science **362**, 65 (2018).

[42] P. Wang *et al.*, *Landau quantization and highly mobile fermions in an insulator*, Nature (London) **589**, 225 (2021).

[43] N. F. Mott and E. A. Davis, *Electronic Processes in Non-Crystalline Materials* (Oxford University Press, New York, 2012).

[44] H. Qiu *et al.*, *Hopping transport through defect-induced localized states in molybdenum disulphide*, Nat. Commun. **4**, 2642 (2013).

[45] B. Shklovskii and A. Efros, *Electronic Properties of Doped Semiconductors* (Springer-Verlag, Berlin, 1984).

[46] C. O. Yoon, M. Reghu, D. Moses, and A. J. Heeger, *Transport near the metal-insulator transition: Polypyrrole doped with* PF_6, Phys. Rev. B **49**, 10851 (1994).

[47] R. M. Hill, *Hopping conduction in amorphous solids*, Philos. Mag. **24**, 1307 (1971).

[48] D. Yu, C. Wang, B. L. Wehrenberg, and P. Guyot-Sionnest, *Variable range hopping conduction in semiconductor nanocrystal solids*, Phys. Rev. Lett. **92**, 216802 (2004).

[49] A. S. Dhoot, G. M. Wang, D. Moses, and A. J. Heeger, *Voltage-induced metal-insulator transition in polythiophene field-effect transistors*, Phys. Rev. Lett. **96**, 246403 (2006).

[50] Y. Aharonov and J. Anandan, *Phase change during a cyclic quantum evolution*, Phys. Rev. Lett. **58**, 1593 (1987).

[51] M. Cheng *et al.*, *Quantum tunneling with tunable spin geometric phases in van der waals antiferromagnets*, Nat. Phys. (2024), 10.1038/s41567-024-02675-x.

[52] X. Lin *et al.*, *Positive oscillating magnetoresistance in a van der Waals antiferromagnetic semiconductor*, arXiv:2410.17930.

[53] Y. Peng *et al.*, *Magnetic structure and metamagnetic transitions in the van der Waals antiferromagnet* $CrPs_4$, Adv. Mater. **32**, 2001200 (2020).

[54] Z. Wang, C. Tang, R. Sachs, Y. Barlas, and J. Shi, *Proximity-induced ferromagnetism in graphene revealed by the anomalous Hall effect*, Phys. Rev. Lett. **114**, 016603 (2015).